AERO-ACOUSTIC ANALYSIS WITH A PERMEABLE SURFACE FOR TIP-JET ROTOR NOISE CHARACTERISTICS IN HOVERING FLIGHT

Kiro Kim[1], Min Jun Park[2], Daun Park[1], Soo Hyung Park[1], Duck Joo Lee[2]

[1] Department of Aerospace Information System Engineering, Konkuk University, Seoul, Rep. of Korea
[2] Department of Aerospace Engineering, Korea Advanced Institute of Science and Technology, Daejeon, Rep. of Korea

Abstract
This paper presents aero-acoustics in far-field computed by an acoustic analogy code using numerical permeable surfaces for the Tip-jet 80-inch model rotor blade in hovering flight. A chimera grid method is applied to the present simulation to consider the blade motion and moving effects. The permeable surface covering the blade and jet flow is constructed to include the thickness noise, loading noise and the flow noise generated from the shock waves, tip vortices and ejected jet. The Kirchhoff approach is applied to Ffowcs Williams and Hawkings (FW-H) equations to efficient noise prediction in far-field. High speed impulsive noise due to blade tip shock waves and jet flow with large pressure gradient is predicted. Noise characteristics in far-field are investigated with jet flow parameters such as duct inlet pressure and total pressure.

1. INTRODUCTION

As the application range of the helicopter has increased not only for military purpose but also for the civilian purpose, a new concept of rotor systems and compound helicopters has been focused on to overcome limitations of conventional helicopters [1]. Compound helicopters have advantages in mission performance because they can operate at relatively high speed compared to conventional helicopters. Among the compound helicopters, the tip-jet rotors deliver compressed air or exhaust gas from the engine to wing tip and rotate the rotor blades by the ejection force from the mounted nozzle. Due to the high-pressure jet flow emitted from the nozzle in the blade tip, complex aerodynamic characteristics may appear compared to conventional helicopters, and it has a significant influence on the performance of the rotor [2]. The issue of noise in the tip-jet rotors, therefore, is recognized as a major disadvantage of tip-jet rotors, and it is essential to accurately predict the aerodynamic noise in the far-field generated from a tip-jet rotor.

Generally, helicopter noise can be divided into thickness noise, loading noise including BVI (Blade-Vortex Interaction) noise, and non-linear noise including HSI (High-Speed Impulsive) noise. Methods for predicting noise include CAA (Computational Aero-Acoustics), which is directly computed using high-order accuracy numerical techniques, and acoustic analogy [3, 4], which numerically computes distant noises using noise source information. The acoustic analogy is widely used to predict far-field noise considering the computational efficiency. BVI noise can be predicted by far-field noise using sound pressure information on the blade surface [5]. HSI noise requires volume integration for the sound pressure information in the flow field to predict the flow noise emitted in the volume grid, which can be predicted by the far-field noise [6]. However, in the view of computational efficiency, the volume integration takes a long time to compute compared to the surface integral. To improve the computational efficiency, di Francescantonio et al [7]. proposed a Kirchhoff approach to Fw-H (Ffowcs Williams and Hawkings) equation. Lyrintzis et al [8]. and Aoyama et al [9]. predicted HSI noise around a rotating rotor using Kirchhoff's equation with a virtual moving control surface. And Brentner et al [10]. showed that FW-H equations are more robust by comparing the volume noise sources with the permeable surface boundary conditions according to FW-H and Kirchhoff equations. Mankabadi et al [11]. analyzed the supersonic jet noise using CFD (Computational Fluid Dynamics) analysis. Brentner et al [12]. classify the noise source of Fairey Rotordyne aircraft as rotational noise and jet noise based on the empirical prediction scheme.

In this study, aero-acoustics in far-field is computed by an acoustic analogy code using the permeable surface for the Tip-jet 80-inch model rotor blade [2] in hovering flight. The prediction method is also demonstrated using 1/7 scaled UH-1H rotor blade. A chimera grid method is applied to the present simulation to consider the blade motion and moving effects. The permeable surface covering the blade and jet flow is constructed to include the thickness noise, loading noise and the flow noise generated

Presented at 44th European Rotorcraft Forum, Delft, The Netherlands, 19-20 September, 2018

from the shock waves, tip vortices and ejected jet. The Kirchhoff approach is applied to FW-H (Ffowcs Williams and Hawkings) equations to efficient noise prediction in far-field. HSI noise and quadrupole noise due to blade tip shock waves with large pressure gradient and jet flow, respectively, were predicted. Noise characteristics in far-field were investigated with jet flow parameters such as duct inlet pressure and total pressure.

2. ANALYSIS METHODOLOGIES

2.1. Grid system and Boundary conditions

The 1/7-scaled UH-1H rotor blade geometry is used to validate the CFD-CAA coupling code. Aerodynamic noise analysis for the Tip-jet 80-inch model rotor blade is performed with different jet flow characteristics.

The chimera grid method is applied to perform aerodynamic analysis. The chimera grid system overlaps each grid system (main grid and sub-grid) and exchanges information between the grids through interpolation points [13]. Therefore, it is easy to generate different grids and to analyze the aerodynamic force with time change for an object having relative motion.

As shown in Table 1, the chimera grid system is generated for the 1/7 scaled UH-1H rotor blade and the Tip-jet 80-inch model rotor blade. Table 2 shows the constructed chimera grid information, and Figure 1 shows each chimera grid.

Table 1. Characteristics of the UH-1H rotor blade and the Tip-jet 80-inch model rotor blade

Case	Airfoil	Planform	Number of blade	Blade radius [m]	Chord length [m]
1/7 scaled UH-1H	NACA0012	Rectangular Non-twisted	2	1.045	0.0762
Tip-jet 80-inch model	Elliptic airfoil	Rectangular Non-twisted	2	1.0145	25% span: 0.20193 93% span: 0.13716

Table 2. Grid information

Case	Grid	Index points normal(i) X spanwise(j) X chordwise(k)	Total cells
1/7 scaled UH-1H	Background	161 X 169 X 241	6,451,200
	Sub grid for 1 blade	49 X 97 X 337	1,548,288
Tip-jet 80-inch model	Background	505 X 189 X 231	21,792,960
	Sub grid for 1 blade	81 X 209 X 257	4,259,840
	Duct	81 X 65 X 49	245,760

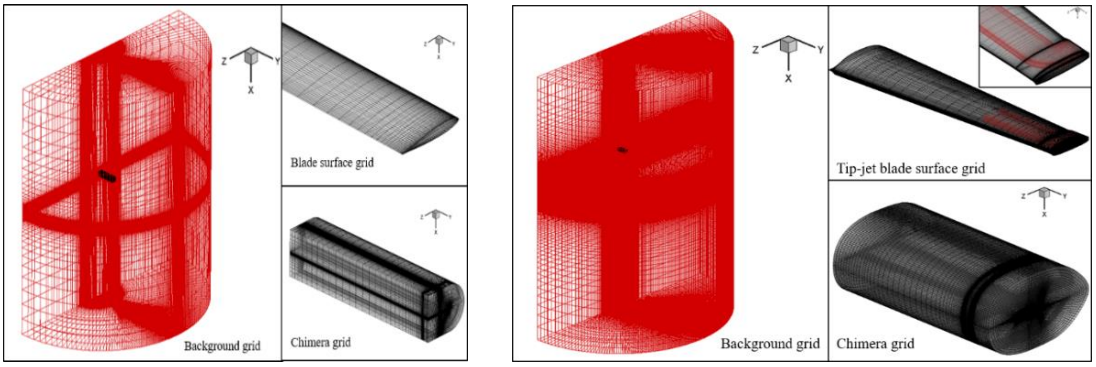

Figure 1. Chimera grid system: 1/7 scaled UH1-H rotor blade(left), Tip-jet 80-inch model rotor blade (right)

Presented at 44th European Rotorcraft Forum, Delft, The Netherlands, 19-20 September, 2018

The duct of Tip-jet rotor is rectangular type, 0.07315 m in width, 0.01341 m in height, and 0.000492 m^2 in nozzle area. More detailed information is given in reference [2]. The first cell spacing in the normal direction is set to 1.0×10^{-5} to calculate the Navier-Stokes equation so that the dimensionless distance y^+ of the first grid point on the wall is close to 1 considering the Reynolds number.

As the boundary condition, adiabatic viscous wall condition is applied to the blade surface, and Riemann invariant condition is applied to the far-field. Both the UH-1H rotor and the Tip-jet 80-inch model rotor consist of two blades. The blade grid is constructed for one blade because of the hovering flight condition. Hence, the periodic interface condition is applied as a boundary condition for the rotation axis interface and the convergence of numerical results is improved through steady-state aerodynamic analysis.

It is important to set the boundary conditions for the jet flow to compute the aerodynamic noise analysis for the tip-jet rotor. To analyze the jet flow in which the inflow is subsonic, the duct inlet boundary condition for fixing the total pressure and the total temperature is set considering the direction of Riemann invariants. In other words, the velocity of the jet flow is calculated by specifying p_t / p_∞ and T_t / T_∞, and extrapolating p, R^+, H_t, and finally updating $\rho, \vec{U}$ [19].

2.2. Permeable Surface

In the noise analysis, the volume noise source is generally predicted as the far-field noise by volume integration of the sound pressure information about the flow field inside the volume grid. However, the volume integration has a disadvantage of the computational efficiency is not good. On the other hand, if the permeable surface (Kirchhoff surface) approach is used, sound pressure information can be delivered to an arbitrary permeable surface so that the far-field noise can be predicted only by the surface integral, and the computational efficiency can be improved.

The permeable surface is constructed to include the physical blade surface and the volume in the flow field where the noise source is located as shown in Figure 2. The position of the permeable surface is set equal to the ratio (z/c) of the chord length (c) to the height, distance (z) in the both of spanwise and chordwise direction from the blade surface. The acoustic pressure at a fixed point is computed by integrating flow solutions obtained at each node point of the permeable surface.

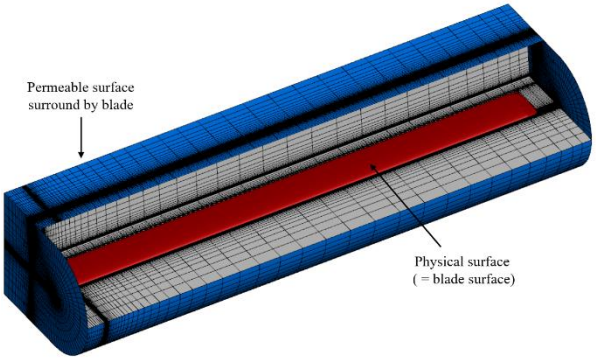

Figure 2 A concept of a permeable surface

2.3. Governing Equations

2.3.1. Aerodynamic analysis

RANS code with three-dimensional compressible Navier-Stokes equations is used to analyze the flow field around the rotor blade. The three-dimensional compressible Navier-Stokes equations in terms of conservation form in the general coordinate system for a hovering rotor blade are written as:

$$\frac{\partial Q}{\partial t}+\frac{\partial (F_i - F_{vi})}{\partial \xi}=S, \qquad i=1,2,3. \tag{1}$$

where, Q is the flow variable, and F_i is inviscid fluxes and F_{vi} is the viscous fluxes in each direction. The flow in the coordinate system fixed to the blade in hovering can be a steady state.

The z-coordinate rotational source term (S), which converts the equations to steady state, is expressed on the right-hand side in Eq. (1). S is written as:

$$S=[0, \rho v\Omega, -\rho v\Omega, 0, 0] \tag{2}$$

where, Ω is the angular velocity of rotating coordinate system. The contravariant velocity is written as:

$$U=\xi_x u+\xi_y v+\xi_z w-\xi_t \tag{3}$$

where, ξ_t is the moving speed applying the rotation of the grid in the ξ direction. The cell-centered finite volume method is used for spatial discretization. The viscous flux is calculated by Roe's FDS (Flux Difference Splitting) scheme [15]. 3rd order TVD (Total Variation Diminishing) interpolation [16] as a limiter is applied for the second-order accuracy. Steady state solutions are

Presented at 44th European Rotorcraft Forum, Delft, The Netherlands, 19-20 September, 2018

obtained by using DADI (Diagonalized Alternate Directional Implicit) method [17] as a time advancing method. $k-\omega SST$ (Shear Stress Transport) model [18] as a turbulence model is used to calculate the flow around rotor blades. And the data of the steady state aerodynamic analysis for the permeable surface is transformed to the results of the unsteady analysis according to the time advance.

2.3.2. Acoustic analysis

FW-H equation with the permeable surface boundary condition is used for the acoustic analysis using Farassat formulation 1A [19]. It is defined by di Francescantonio [7], which applies Eq. (4) and Eq. (5). it provides the permeable surface boundary condition $(u_n \neq v_n)$ with an arbitrary virtual surface to the impermeable surface boundary condition $(u_n = v_n)$ to calculate the sound field on the blade surface.

(4) $$U_i = [1-(\rho/\rho_0)]v_i + (\rho/\rho_0)u_i$$

(5) $$L_i = P_{ij}n_j + \rho u_i(u_n - v_n)$$

The integral form can be written as following Eq. (6) to Eq. (8)

(6) $$p'(\vec{x},t) = p'_T(\vec{x},t) + p'_L(\vec{x},t) + p'_Q(\vec{x},t)$$

(7)
$$p'_T = \frac{1}{4\pi}\int_{f=0}\left[\frac{\rho_0(\dot{U}_n + U_{\dot{n}})}{r\left|1-M_r\right|^2}\right]_{ret} ds + \frac{1}{4\pi}\int_{f=0}\left[\frac{\rho_0 U_n(r\dot{M}_r + cM_r - cM^2)}{r^2\left|1-M_r\right|^3}\right]_{ret} ds$$

(8)
$$p'_L = \frac{1}{4\pi c}\int_{f=0}\left[\frac{\dot{L}_{\dot{n}}}{r\left|1-M_r\right|^2}\right]_{ret} ds + \frac{1}{4\pi c}\int_{f=0}\left[\frac{L_r - L_i M_i}{r^2\left|1-M_r\right|^2}\right]_{ret} ds + \frac{1}{4\pi c}\int_{f=0}\left[\frac{L_r(r\dot{M}_r + cM_r - cM^2)}{r^2\left|1-M_r\right|^3}\right]_{ret} ds$$

where, $n = n_i$ is the unit normal vector component outward to the blade surface. $u_n = u_i n_i$ is the flow velocity component normal to the blade surface and $v_n = v_i n_i$ is the surface velocity component normal to the blade surface. $\rho = \rho_0 + \rho'$ is density variation and $r = \left|\vec{x} - \vec{y}\right|$ is the distance between the blade surface and the observer location. M and $M_r = M_i r_i$ are local Mach number on the blade surface and Mach number of the source in radiation direction, respectively. In Eq. (7), $p'_T(\vec{x},t)$, $p'_L(\vec{x},t)$, $p'_Q(\vec{x},t)$ denotes the thickness, the loading, and the volume noise term, respectively.

To solve Eq. (7), the need to integrate the entire volume makes computational efficiency poor. However, applying Eqs. (5) and (6) with the permeable surface boundary condition, the volume noise source can be included in Eqs. (8) and (9). Therefore, it is possible to increase the calculation efficiency by using only the surface integral, and it is also possible to predict all the noise sources (monopole, dipole, quadrupole).

3. NUMERICAL RESULTS

3.1. CFD-CAA coupling code validation with 1/7 scaled UH-1H rotor blade model

To demonstrate a capability of the present CFD-CAA coupling code, the aerodynamic noise analysis is carried out under the flow condition of tip Mach number 0.88 where strong shock waves are generated using the 1/7 scaled UH-1H rotor blade.

All noise sources are predicted at the 3.09 R (Blade radius) position of the observer from the center of the rotation plane. The flow information needed to calculate the acoustic pressure at every moment is generated at $dt = 0.152307\times10^{-4}$ intervals corresponding to 0.25 degrees in azimuth angle.

The results of the aerodynamic noise analysis with the different permeable surface locations (z/c = 0.076, 0.35, 0.5, 1.0, 1.5) is validated and compared with those of Brentner et al [10]. and the experimental results [20].

Figure 3 shows the results of the aerodynamic noise analysis with each permeable surface location. The position of the applied permeable surface together with the pressure distribution results is shown in Figure 3(a). The results of the noise analysis with the permeable surface position set to z/c = 0.076, 0.35, and 0.5 are shown in Figure 3(b). When the permeable surface location is close to the blade surface such as z/c = 0.076, 0.35, and 0.5, there is a difference in the acoustic pressure because the shock waves generated from the blade tip is not completely contained as shown in Figure 3(a).

Presented at 44th European Rotorcraft Forum, Delft, The Netherlands, 19-20 September, 2018

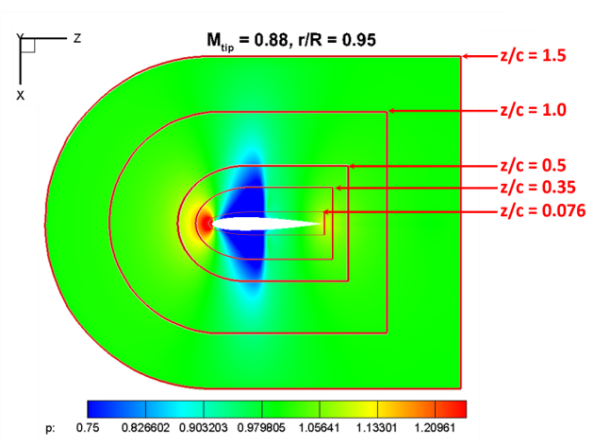

(a) Permeable surfaces location

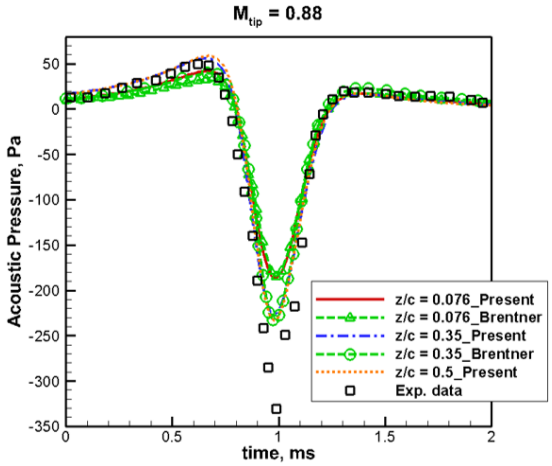

(b) Acoustic pressure with z/c = 0.076, 0.35, 0.5

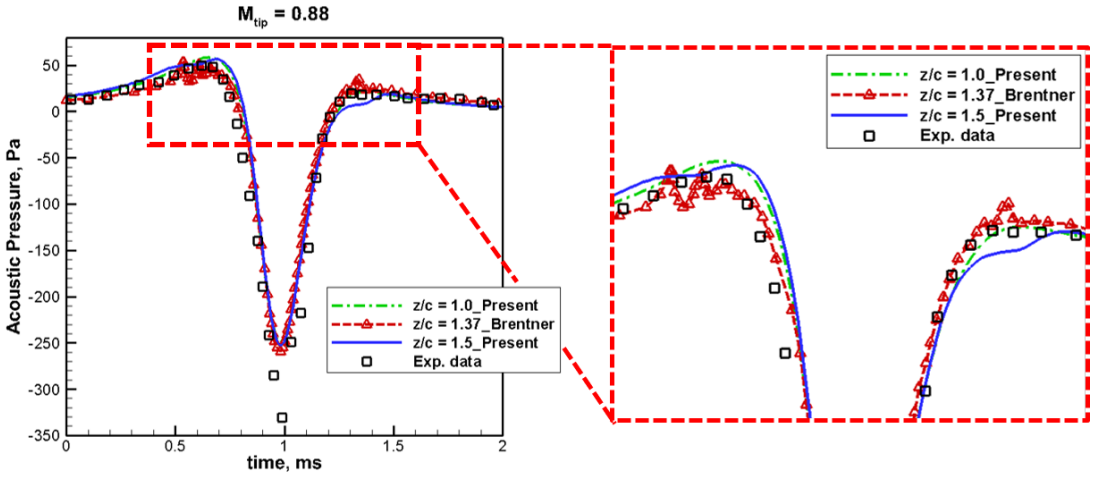

(c) Acoustic pressure with z/c = 1.0, 1.5

Figure 3. Comparison of rotor noise analysis for different permeable surfaces location(z/c)

Figure 3 (c) shows the results of noise analysis for the permeable surface positions of z / c = 1.0 and 1.5. The present results are very similar to the those of Brentner et al [10]. and the peak value of the acoustic pressure appears closer to the experimental results [20] in the case of the permeable surface which completely covers the shock waves. It implies that the large pressure gradient by the shock waves is the most dominant factor of determining the intensity of the sound pressure in the far-field noise prediction. Therefore, it is important that the permeable surface should completely contain the flow information such as HSI noise source by the shock waves and the other large pressure gradient to help predict more accurate the volume noise sources.

It is interesting that, in Brentner et al [10]. case, there is a small oscillation of the acoustic pressure at time = 0.5~0.7 and 1.25~1.4 as shown in Figure 3(c). In contrast, the numerical results of the present study yielded linear acoustic pressure results without any oscillation. It should be noted that the noise analysis is performed with the steady state flow solution. The fully converged flow solution has a much smaller error than that produced from the unsteady aerodynamic analysis. As a result of the analysis using the 1/7 scaled UH-1H rotor blade, the volume noise including the thickness noise and the loading noise was accurately predicted. Especially, it is found that the HSI noise source by the shock wave is accurately predicted, and the accuracy and reliability of the present CFD-CAA coupling code are demonstrated by showing similar results with the previous research results and the experimental results.

3.2. Tip-jet 80-inch model rotor case

Based on the validation of the present code, the aerodynamic noise analysis is computed for the Tip-jet 80-inch model blade.

Figure 4 shows the Tip-jet 80-inch model rotor

Presented at 44th European Rotorcraft Forum, Delft, The Netherlands, 19-20 September, 2018

blade shape and the duct inside the blade. The Tip-jet 80-inch model rotor blades are designed to rotate both clockwise and counter-clockwise with the nozzle located at both the front and rear side of the blade [2]. In this study, the rotation in the clockwise direction is considered, and the position of the nozzle exit is set to be located only in the trailing edge. Also, the duct flow analysis is computed from the position of 70% of the rotor blade radius for considering the calculation efficiency as described in Figure 4.

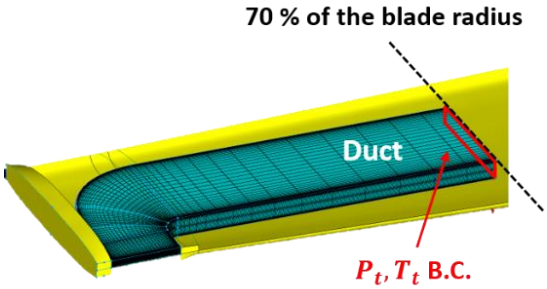

Figure 4. Inside of the tip-jet rotor blade

Tip Mach number is set to 0.358(= 400 ft/s = 121.92 m/s) and collective pitch angles are 0 and 4 degrees. The aerodynamic noise characteristics of the ducts were investigated and compared by varying the duct inlet pressure 1.2 times, 1.4 times, 1.8 times, and 2 times to the atmospheric pressure Figure 9 represents the present results compared to the experimental results [7] with the drive torque of the tip-jet rotor for different the atmospheric pressure to duct inlet pressure ratios (P_{inlet} / P_{atm}) when the collective pitch angle is 0 degree. It is found that as the duct inlet pressure increases, the drive torque increases linearly.

The accuracy of the aerodynamic analysis on the tip-jet rotor geometry was verified by the analysis of the flow inside the duct, which showed an average error of 2.78%.

In the Tip-jet rotor case, all noise sources are predicted at the 3.0 R (Blade radius) position of the observer from the center of the rotation plane. The flow information needed to calculate the acoustic pressure at every moment is generated at $dt = 0.725957 \times 10^{-4}$ intervals corresponding to 0.5 degrees in azimuth angle.

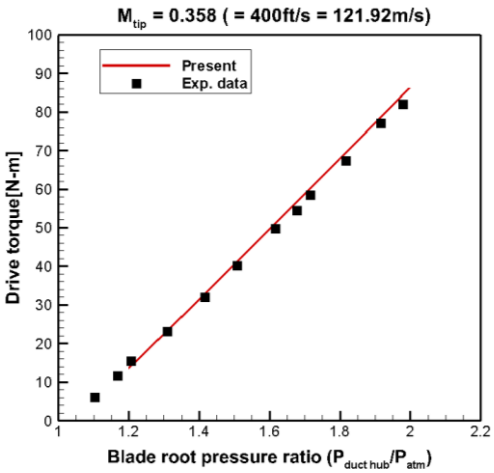

Figure 5. Drive torque to the different blade root pressure ratios

Figure 6 and Figure 7 show the pressure coefficient value at the 95% span and the results of the noise analysis for various observer positions according to the collective pitch angles, respectively.

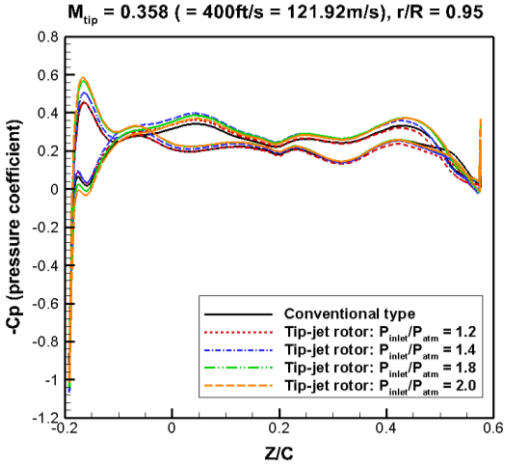

(a) Collective pitch angle 0°

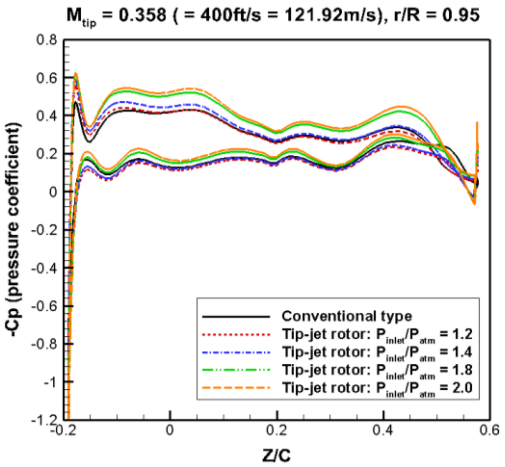

(b) Collective pitch angle 4°

Figure 6. Comparison of pressure coefficient for different nozzle inlet pressure ratios at 95% span

Presented at 44th European Rotorcraft Forum, Delft, The Netherlands, 19-20 September, 2018

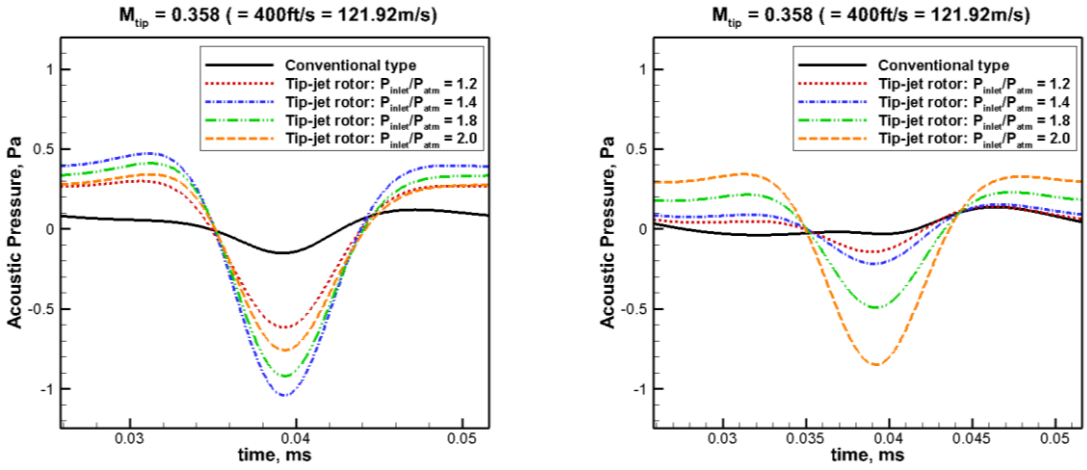

(a) Acoustic pressure at collective pitch angle 0° (b) Acoustic pressure at collective pitch angle 4°

Figure 7. Comparison of tip-jet rotor noise for different nozzle inlet pressure ratios

Table 3. Computed OASPL (dB) values for different nozzle inlet pressure ratios at collective pitch angle 0 degree

Tip-jet Noise	Value (dB)
Conventional type	71.9
$P_{inlet} / P_{atm} = 1.2$	82.6
$P_{inlet} / P_{atm} = 1.4$	86.4
$P_{inlet} / P_{atm} = 1.8$	84.5
$P_{inlet} / P_{atm} = 2.0$	83.4

Table 4. Computed OASPL (dB) values for different nozzle inlet pressure ratios at collective pitch angle 4 degrees

Tip-jet Noise	Value (dB)
Conventional type	73.2
$P_{inlet} / P_{atm} = 1.2$	76.3
$P_{inlet} / P_{atm} = 1.4$	77.3
$P_{inlet} / P_{atm} = 1.8$	80.9
$P_{inlet} / P_{atm} = 2.0$	84.5

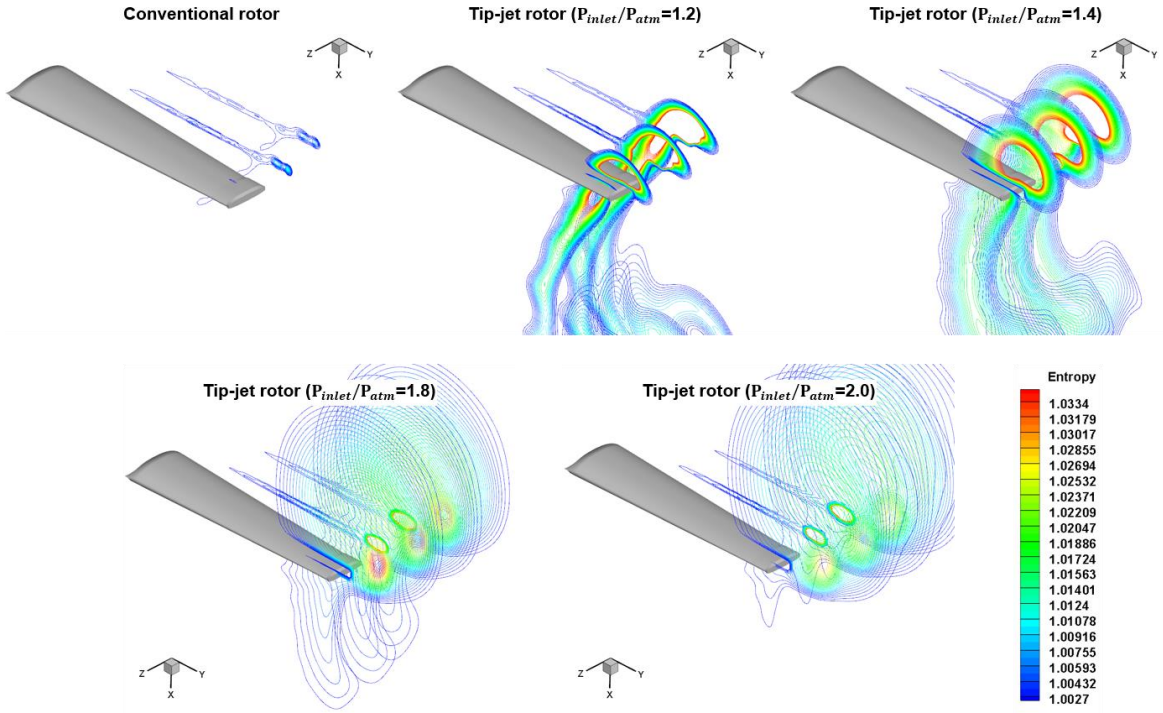

(a) Collective pitch angle 0°

Presented at 44th European Rotorcraft Forum, Delft, The Netherlands, 19-20 September, 2018

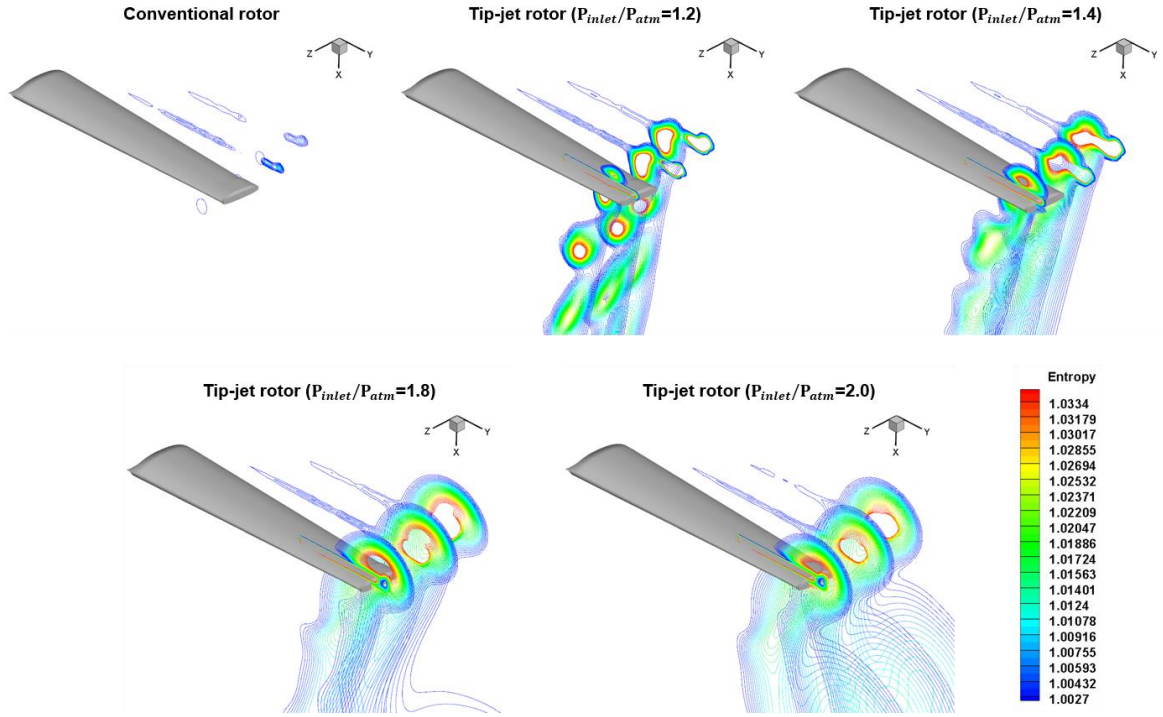

(b) Collective pitch angle 4°

Figure 8. Comparison of computed entropy contour for different nozzle inlet pressure ratios

In the case of collective pitch angle of 0 degree, as the pressure ratio increase, the acoustic pressure does not increase linearly as shown in Figure 7(a). The reason is that the vortex was captured on the blade tip surface at pressure ratios of 1.2 and 1.4, and the vortex with greater strength was predicted at 1.4 as shown in Fig. 8(a).

In the conventional type rotor blade case, the vortex is captured on the blade tip surface. But there is no tip-jet nozzle so that the vortex strength is relatively weak and there is no tip-jet nozzle. Therefore, turbulent noise source due to jet flow did not occur and the total acoustic pressure value is predicted to be low. In contrast, the characteristics of the tip vortex generated on the blade surface under the pressure ratios 1,8 and 2.0 appears differently as shown in Figure 8(a). It implies that the vortex diffuses outward from the blade tip due to the relatively strong jet flow, which weakens the jet-vortex interaction. For this reason, at pressure ratios of 1.8 and 2.0, the pressure gradient around the blade is relatively low compared to the pressure ratio of 1.4, so the acoustic pressure is predicted to be low. Hence, it is found that jet-vortex interaction is an important factor for increasing the noise. The computed OASPL value in Table 3 indicates that tip-jet noise is about 14.5 dB louder at a pressure ratio of 1.4 compared to the conventional type rotor without the nozzle.

On the contrary, in the case of the collective pitch angle of 4 degrees, the acoustic pressure increases as the pressure ratio increase. As shown in Figure 8(b), the tip vortex is also captured. However, its size and strength are weaker than those of the collective pitch angle of 0 degree. It is considered that the tip vortex rapidly diffuses due to the jet flow which is strongly ejected below the rotational plane. Hence, as the pressure ratio increases, the pressure gradient around the blade also increases, so that the acoustic pressure is predicted to be high. The computed OASPL value in Table 4 shows that tip-jet noise is about 14.5 dB louder at the pressure ratio of 1.4 compared to the conventional type.

Consequently, the jet flow-tip vortex interaction is a significant factor to determine the far-field noise characteristics for the tip-jet rotor.

4. CONCLUSION

In this study, the validation of the present CFD-CAA coupling code with the permeable surface was carried out using 1/7 scaled UH-1H rotor blade. And the noise characteristics in far-field of the Tip-jet 80-inch model rotor was numerically investigated with the various jet flow parameters such as the nozzle inlet pressure and total

Presented at 44th European Rotorcraft Forum, Delft, The Netherlands, 19-20 September, 2018

pressure.
To accurately predict far-field acoustic noise, the permeable surface should be constructed to cover the shock waves completely. Also, it is important to use fully-converged flow field solutions to minimize the numerical errors.
Results of the aerodynamic noise analysis for the Tip-jet 80-inch model rotor show that unique noise signature was presented by the effect of the jet flow-tip vortex interaction.
It is found that all noise sources such as HSI noise and jet-vortex interaction of the tip-jet rotor blades can be predicted using the present CFD-CAA coupling code. Therefore, the present methodology will be useful as a framework of parameter studies for the noise reduction in the early stage of the tip-jet rotor design.

5. ACKNOWLEDGMENTS

This work was conducted at High-Speed Compound Unmanned Rotorcraft (HCUR) research laboratory with the support of Agency for Defense Development (ADD).

6. REFERENCES

[1] M. J. Hirschberg, “An Overview of the History of Vertical and/or Short Take-Off and Landing (V/STOL) Aircraft”, CENTRA Technology, Inc., www.vstol.org, 2006.
[2] A. W. Schwartz, “Tipjet 80-Inch Model Rotor Hover Test: Test No. 1198,” Ship Systems Directorate, Research and Development Report, Carderock Division, Naval Surface Warfare Center, Bethesda, 1993.
[3] J. Michael, “On sound generated aerodynamically. II. Turbulence as a source of sound,” Lighthill, Proceedings of the Royal Society of London. Series A, Mathematical and Physical Sciences, 1954, pp. 1~32.
[4] J. F. Williams, and L. H. David, “Sound generation by turbulence and surfaces in arbitrary motion,” Philosophical Transactions of the Royal Society of London A: Mathematical, Physical and Engineering Sciences, Vol. 264, No. 1151, 1969, pp. 321~342.
[5] S. Y. Wie, D. K. Im, J. H. Kwon, D. J. Lee, K. H. Chung, and S. B. Kim, "Helicopter rotor noise in the merged tip-vortex and blade interaction condition," International Journal of Aeroacoustics, Vol.10, No.4, 2011, pp.427-442.
[6] F. Farassat, “Quadrupole source in prediction of the noise of rotating blades-A new source description,” American Institute of Aeronautics and Astronautics Conference, 1987.
[7] P. Di Francescantonio, “A new boundary integral formulation for the prediction of sound radiation,” Journal of Sound and Vibration, Vol. 202, No. 4, 1997, pp. 491~509.
[8] A. S. Lyrintzis, Y. Xue, and S. Anastasios, “The use of Kirchhoff’s method in computational aeroacoustics,” Journal of Fluids Engineering, Vol. 116, No. 4, 1994, pp. 665~676.
[9] T. Aoyama, K. Kawachi, S. Saito, and J. Kamio, “Unsteady analysis of transonic helicopter rotor noise,” 19th European Rotorcraft Forum, 1993.
[10] K. S. Brentner, and F. Farassat, “Analytical comparison of the acoustic analogy and Kirchhoff formulation for moving surfaces,” AIAA journal, Vol. 36, No. 8, 1998, pp. 1379~1386.
[11] R. R. Mankbadi, M. E. Hayder, and L. A. Povinelli, “The Structure of Supersonic Jet Flow and Its Radiated Sound,” AIAA Journal, Vol. 32, No. 5, 1994, pp. 897~906.
[12] K. S. Brentner, P. J. Morris, and L. V. Lopes, “A method for predicting the noise of a tip-jet driven rotor,” Journal of the American Helicopter Society, Vol. 59, No. 3, 2014, pp. 1~10.
[13] D. K. Im, S. Y. Wie, E. Kim, J. H. Kwon, D. J. Lee, S. H. Park, K. H. Chung, and S. B. Kim, “Unsteady Aerodynamic Analysis for Helicopter Rotor in Hovering and Forward Flight Using Overlapped Grid,” Journal of The Korean Society for Aeronautical and Space Sciences, Vol. 37, No. 3, 2009, pp. 215~223.
[14] J. R. Carlson, “Inflow/outflow boundary conditions with application to FUN3D,” 2011, NASA
[15] P. L. Roe, “Approximate Riemann Solvers, Parameter Vectors, and Difference Schemes,” Journal of computational physics, Vol. 2, No. 43, 1981, pp. 357~372.
[16] K. H. Kim, and C. Kim, “Accurate, Efficient and Monotonic Numerical methods for Multi-dimensional Compressible Flows Part II: Multi-dimensional Limiting Process,” Journal of Computational Physics, Vol. 208, No. 2, 2005, pp. 570~615.
[17] S. H. Park, and J. H. Kwon, “Implementation of k-w Turbulence Models in an Implicit Multigrid Method,” AIAA journal, Vol. 7, No. 42, 2004, pp. 1348~1357.
[18] F. R. Menter, “Two-Equation Eddy- Viscosity Turbulence Models for Engineering Applications,” AIAA Journal, Vol. 32, No. 8, 1994, pp.1598~1605.
[19] F. Farassat, and P. S. George “The prediction of helicopter rotor discrete frequency noise,” 38th American Helicopter Society Annual Forum, Proceedings. (A82-40505 20-01), 1982, pp. 497~507.
[20] T. W. Purcell, “CFD and transonic helicopter sound,” 14th European Rotorcraft Forum, 1988, pp.17.

Presented at 44th European Rotorcraft Forum, Delft, The Netherlands, 19-20 September, 2018